Control of Linear Motors for Machine Tool Feed Drives: Design and Implementation of H_∞ Optimal Feedback Control[1]

D. M. Alter[2]

Tsu-Chin Tsao

Department of Mechanical and Industrial Engineering, University of Illinois at Urbana-Champaign, Urbana, IL 61801

Direct drive linear motors have good potential for use as next generation machine tool feed drives since they can increase machining rates and improve servo accuracy by eliminating gear related mechanical problems. To exploit the high speed and high response direct drives for machining, the servo control must achieve as high as possible tracking performance while at the same time establishing as much as possible the dynamic stiffness in order to maintain machining stability and reduce the effect of machining disturbance forces on the tool position. This paper investigates the use of optimal H_∞ control to design for large stiffness and closed-loop tracking performance. Position feedback alone is first considered, with cutting force feedback later added to augment closed loop stiffness. Optimal position feedback is experimentally seen to achieve up to a 46 percent stiffness improvement over that achievable with proportional-derivative control. The addition of force feedback to the servo-loop resulted in a further 70 to 100 percent stiffness improvement over the position feedback alone values.

1 Introduction

Direct electric feed drives have come under study relatively recently for use in next generation high-speed machine tools. Directly driven feed axes eliminate gear related mechanical problems such as backlash, large frictional and inertial loads, and structural flexibilities and therefore have the potential to increase machining speed and accuracy. However, there exists a strong dynamic feedback interaction between the machining process and the direct drives which can lead to excessive vibration or self-excited chatter instability. Chatter and vibration leave ripple marks and indentations on the workpiece which degrade surface finish, and can even cause tool breakage. Without servo-feedback control the direct feed drives do not have stiffness to maintain machining stability. Therefore, to exploit the high speed and high response direct linear drives for machining applications, the servo-control must achieve as high as possible the tracking performance while at the same time establishing as much as possible the dynamic stiffness in order to maintain machining stability and reduce the effect of machining disturbance forces on the tool position. This paper addresses the dynamic stiffness of these two issues.

Chatter instability in directly driven machining systems has been previously investigated, and various necessary and sufficient stability conditions have been developed (Srinivasan and Nachtigal, 1978; Alter and Tsao, 1994). Figure 1 shows the system block diagram employed in these studies, here in a slightly simplified form. The cutting process dynamics from depth of cut (d_{cut}) to cutting force (F_c) are denoted by $G_{cp}(\cdot)$, and may be both nonlinear and time-varying in nature. The machine tool/workpiece structural dynamics from cutting force input to (workpiece) position output (y_w) are denoted by $G_{mw}(s)$, and the drive motor dynamics from force input to position output (y) are denoted by $P(s)$. Note that tool post dynamics may be embedded in $P(s)$ if it is desired to do so. The servo-controller $C_{fb}(s)$ produces a force input command to the motor using the position error signal as its input, where r represents the desired motor position.

This diagram is applicable to any general cutting operation (e.g., milling, turning, grinding) were the particular cutting geometry may be defined by the above operator blocks. Note that the variable d_{cut} does not necessarily represent depth of cut in the commonly used sense. For example, if the linear motor is providing feed direction motion for a turning operation, d_{cut} actually represents chip thickness.

Three feedback loops exist in the system: the machine tool/workpiece loop, the feed drive servo-loop, and the outer loop that connects the first two loops. The machine tool/workpiece loop is the traditional machining stability loop considered in the literature (Merritt, 1965), and will be assumed stable in this paper. In addition, this loop will be further neglected by assuming $G_{mw}(s) = 0$, which means that the machine tool/workpiece has relatively large stiffness. Chatter instability can thus only manifest itself in the outer loop. One stability approach is to consider the cutting process as all possible stable perturbations whose L_2 induced system gain is bounded by ρ, i.e.,

$$\sup_{w} \frac{\|G_{cp}(\cdot)w\|_2}{\|w\|_2} < \rho \tag{1}$$

where $w(t)$ is an arbitrary input signal with $0 < \|w\|_2 < +\infty$. Assuming that the servo-loop transfer function y/F_c is stable in the absence of the cutting process, the small gain theorem states that the outer system loop (with the cutting process present) is stable if and only if

$$\left\| \frac{y}{F_c} \right\|_\infty < \frac{1}{\rho} \tag{2}$$

Therefore, a reasonable goal with regards to chatter control is to minimize the H_∞ norm of the servo-loop from force disturbance to position output. This is equivalent to maximizing servo-dynamic stiffness, which is defined as the scalar inverse

[1] This work was supported in part by National Science Foundation, Grant No. DDM-90-09830.

[2] Currently with the Dept. of Mech. Eng., Lafayette College, Easton, PA.

Contributed by the Dynamic Systems and Control Division for publication in the JOURNAL OF DYNAMIC SYSTEMS, MEASUREMENT, AND CONTROL. Manuscript received by the DSCD June 1, 1994. Associate Technical Editor: O. Nwokah.

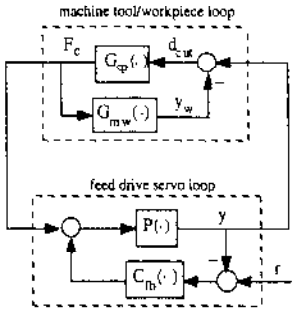

Fig. 1 Machining system block diagram

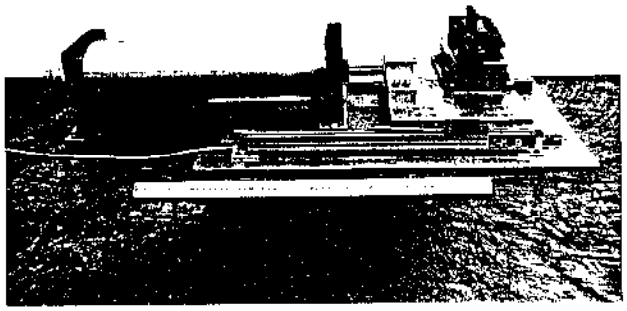

Fig. 3 Photograph of AURA HFA-100/6 linear motor

of the left hand side of (2). By requiring the satisfaction of condition (2), one may now treat the cutting force as an external disturbance to the servo-loop, rather than a signal in a feedback loop.

While stability condition (2) may be conservative for specific machining situations (i.e., when information about the cutting process is known beyond the gain bound ρ), it is a reasonable goal for a general purpose machine tool required to perform different machining operations under various cutting conditions (e.g., depth of cut, spindle speed, material type, tool geometry).

Aside from stability considerations, active control objectives for direct drive machining include designing for disturbance rejection and tracking properties. Machining errors result from the combined effects of cutting force disturbances and servo-loop tracking errors, the later of which would be present even in the absence of the cutting process. Disturbance rejection properties depend upon the same transfer function y/F_c as does the stability condition (2), and further motivates the use of H_∞ optimal control for this problem.

The proposed control structure is depicted in Fig. 2. Three controllers are shown: position feedback (C_{fb}), cutting force feedback (C_{fb}), and tracking feedforward (C_{ff}). The linear motor model is shown with two inputs: the first is the voltage command to the servo amplifier, while the second is the force input to the motor mechanical dynamics. The two plant sections are coupled through a feedback path that will be detailed in the next section. The tracking feedforward controller will be the focus of a subsequent paper, and will not be discussed further here. The two feedback controllers are together tasked with achieving good dynamic servo stiffness.

The rest of this paper is organized as follows. A nominal linear motor drive model is first presented and derived experimentally together with its unmodeled dynamics. Based on the nominal model, the maximum achievable dynamic stiffness with PD position feedback is calculated. The limit of performance for all stabilizing controllers is derived based on H_∞ theory to show the potential room of improvement over PD control. H_∞ controllers that take into account practical considerations such as robust stability, control energy limits, and closed-loop tracking performance are designed and implemented with comparison to the optimal PD controllers. After this, a force feedback controller which utilizes the (cutting) force disturbance measurement is designed and implemented to enhance the stiffness of the position servo loop.

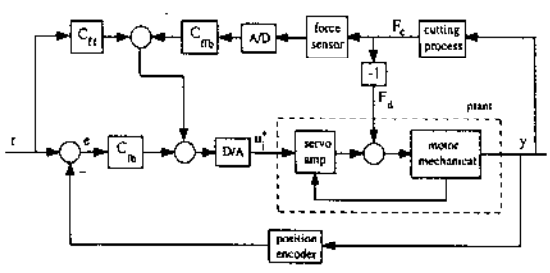

Fig. 2 Controller scheme showing feedback and feedforward controllers

2 System Open Loop Modeling

The hardware used for experimentation in this and the following paper is an AURA HFA-100/6 linear motor powered by an Advanced Motion Controls #40A20 PWM servo-amplifier, shown in the photograph of Fig. 3 (the ruler shown in the picture foreground is 60 cm in length). Mounted on the motor slide is a Kistler 9257A force dynamometer which will be used later to sense cutting force, and mounted on the dynamometer is a tool post. Tool position is measured with an optical encoder of 2 μm resolution mounted to the linear motor slide (in foreground), and controller implementation will be performed by a 32 bit floating-point digital signal processor (TMS320C30) accessed through an IBM-AT host computer.

While PD control may be designed and implemented without the aid of a good open loop dynamic model, one must generate a better model if servo-performance potentials are to be fully realized. In particular, the dynamics of the servo-amplifier could be of great significance if large performance demands are placed on the motor. A fourth-order model is here applied, illustrated in block diagram form in Fig. 4. In addition to the second-order inertial dynamics, this model includes first order dynamics for the motor electrical components (i.e., coil inductance and resistance) and a PI controller for the servo amplifier current loop. The following open loop transfer functions, which naturally share a common denominator, may be obtained from this figure:

$$P_1(s) := \frac{y(s)}{u_i^*(s)} = \frac{K_u C_{w1}(K_{pi}s + K_{ii})}{[L_a s^2 + (R_a + K_{pi}K_i)s + K_{ii}K_i](ms + B) + C_{w1}C_{w2}s} \cdot \frac{1}{s} \tag{3a}$$

$$P_2(s) := \frac{y(s)}{F_d(s)} = \frac{L_a s^2 + (R_a + K_{pi}K_i)s + K_{ii}K_i}{[L_a s^2 + (R_a + K_{pi}K_i)s + K_{ii}K_i](ms + B) + C_{w1}C_{w2}s} \cdot \frac{1}{s} \tag{3b}$$

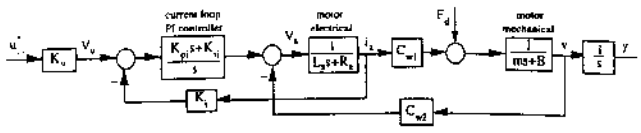

Fig. 4 Open-loop motor block diagram

Table 1 Identified open-loop model parameters

m	B	L_a	R_a	C_{w1}	C_{w2}	K_t	K_a	K_{pa}	K_{ii}
17.40, 27.65 Kg	250 N · s/m	1.6e-3 H	0.7 Ω	34.25 N/A	34.25 V · s/m	0.1855 V/A	0.94 V/V	7.94	0 s^{-1}

Table 1 lists the identified parameter values, which were determined as follows: the system mass (m) was weighed, the damping value (B) was found via frequency response curve fitting techniques, K_a, K_t, K_{pi}, and K_{ii} were found using static gain tests, and the remaining parameters were obtained from the manufacturers documentation (C_{w1}, C_{w2}, L_a, and R_a). The difference between the two listed mass values is the weight of the force dynamometer. Also, the value $K_{ii} = 0$ reflects the fact that the integrating capacitor in the amplifier current loop was intentionally shorted to avoid integral windup in this loop.

Frequency response verification of the overall open-loop model $P_1(s)$ is shown in Fig. 5 for the case of $m = 17.40$ kg (the case of $m = 27.65$ is similar). The experimental frequency response was generated in two pieces: a low frequency band using encoder measurements (<70 Hz), and a high frequency band using an accelerometer sensor. The discontinuity in the experimental curves at 70 Hz is due to mismatch between the two tests, and does not reflect system behavior. Low frequency phase mismatch between experimental and model data may be a result of static friction. Causing high frequency mismatch is a resonance/anti-resonance behavior in the range of 900–1100 Hz (350–500 Hz for the $m = 27.65$ kg case). This has been attributed to mechanical structure flexibility.

Irrespective of the causes, all mismatches between model and experimental frequency responses have been quantified as multiplicative unmodeled dynamics:

$$\hat{P}_1(s) = P_1(s)[1 + \Delta_1(s)] \tag{4}$$

where $\hat{P}_1(s)$, $P_1(s)$, and $\Delta_1(s)$ respectively represent the actual plant, the nominal plant (i.e., modeled dynamics), and the unmodeled dynamics.

The unmodeled dynamics $\Delta_1(s)$ may be computed from (4) on a frequency by frequency basis using the identified nominal model and experimental frequency response data. A magnitude plot of the unmodeled dynamics is shown in Fig. 6 for both mass cases. The largest unmodeled dynamics correspond to those frequencies at which the resonance/anti-resonance behavior occurs. Note that the unmodeled dynamics of $P_2(s)$ will not affect the robust stability of the servo-loop since the cutting force is treated as an external disturbance, and have not been documented in this work. They have only the potential to change the closed loop stiffness.

Since controller design is to be performed in the discrete-time domain, conversion of the continuous-time domain model to a discrete model must be performed. Referring to Fig. 2, it is clear that $P_1(s)$ may be transformed with no approximation using the standard zero-order hold technique. On the other hand, conversion of $P_2(s)$ using this method introduces some error since the external force disturbance F_d is a continuous signal. However, this approximation does not affect system stability if the effects of the zero-order hold are accounted for in (1), and should not greatly compromise closed loop stiffness except possibly in the highest frequency band below the sample rate Nyquist frequency. As such, the (approximate) discrete equivalent model may be written as

$$y(k) = P_1(z)u_i^*(k) + P_2(z)F_d(k) \tag{5}$$

where transfer functions $P_1(z)$ and $P_2(z)$ are the conventional zero-order hold equivalents of $P_1(s)$ and $P_2(s)$ in the Z-transform operator z. Note that $P_1(z)$ and $P_2(z)$ will share a common denominator (i.e., the sampled equivalent of the common denominator of $P_1(s)$ and $P_2(s)$). The reader is referred to (Alter, 1994) for a more extensive and detailed presentation of the system modeling.

3 Achievable Dynamic Stiffness of the Nominal Plant Model

While a practical controller must take into account robustness, control energy, tracking, and possibly other constraints, we first consider the maximum dynamic stiffness achieved by position output feedback control for the nominal linear motor drive model in Eq. (3). This information is useful for understanding the theoretical limit of (dynamic stiffness) performance. PD control and H_∞ optimal control will be considered. While PD control result gives what commercial servo control, which is predominantly PID type, can achieve, the H_∞ optimal control result gives the limit of performance for all the stabilizing feedback controllers.

In view of Eq. (2), the dynamic stiffness for position feedback system can be derived from the inverse of the H_∞ norm of the transfer function

$$\frac{y(z)}{F_d(z)} = \frac{P_2(z)}{1 + P_1(z)C_{fb}(z)}. \tag{6}$$

Discrete PD control has been optimized for maximum dynamic stiffness from this transfer function. A brute-force numerical scheme was used to search over the PD control parameter space:

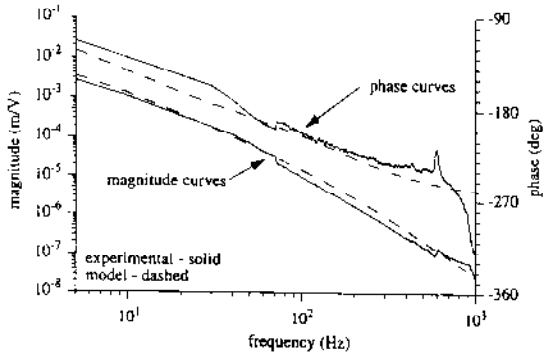

Fig. 5 Open-loop frequency response y/u_i^*, $m = 17.40$ kg

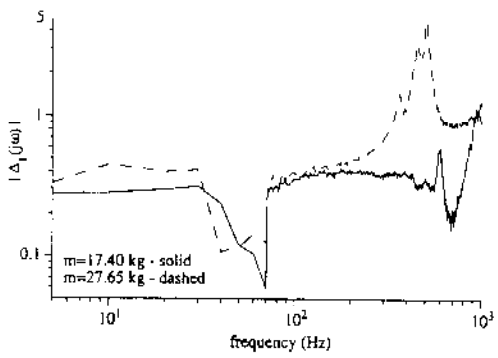

Fig. 6 Unmodeled dynamics of open-loop model $P_1(s)$

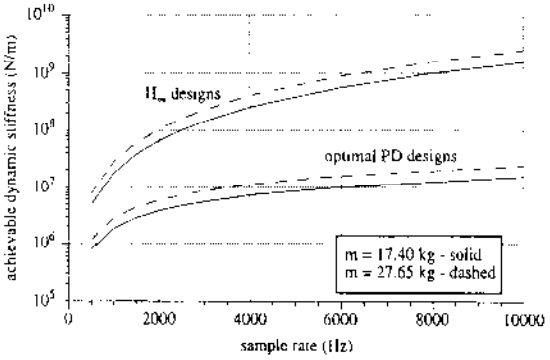

Fig. 7 Theoretically achievable stiffness for H_∞ and PD feedback controllers

$$\text{PD control} \Rightarrow C_{fb}(z) = K\frac{z+b}{z},$$

$$0 < K \le K_{\max}, \quad -1 < b \le 0 \quad (7)$$

where $K_{\max}$ is the maximum gain possible for stability with the particular b value under consideration. Using MATLAB™ software, the optimization was accomplished by simply testing successive values of b between -1 and 0 with a 0.01 interval, determining $K_{\max}$ from the open-loop Nyquist plot for each b, sweeping through the possible values of K using a $0.01 * K_{\max}$ interval, and determining the closed-loop dynamic stiffness for each K from the bode plot. The maximum dynamic stiffness over the search yields the optimal K and b for any particular sampling rate. Figure 7 shows the derived maximum dynamic stiffness for the range of b value at several sampling rates and $m = 17.40$ kg. The maximum stiffness value on each curve is thus the maximum achievable dynamic stiffness for that sampling rate. The plot trends for $m = 27.65$ kg are similar (not shown). From this figure it can be seen that the optimal PD design tends toward pure derivative control ($b = -1$) as sample rate increases, and de-emphasizes the derivative term as sample rate decreases. Also, the stiffness sensitivity to "b" around the optimal b value increases with sampling rate. This is of significance when implementing an optimized PD design: lower sampling rates allow a greater margin of error in the chosen value of b at the expense of lower achievable stiffness.

The limit of performance is derived by finding among all the stabilizing controllers, the maximum closed-loop dynamic stiffness. The setup and solution to such a SISO H_∞ optimization problem is well understood, and in this work the problem has been cast in the standard model matching form via the all-stabilizing controller method (Vidyasagar, 1985), and then solved via simple interpolation (Zames and Francis, 1983). The achievable dynamic stiffness using the nominal model of the linear motor is plotted in Fig. 8 for a range of different sampling rates, and compared to the PD control result.

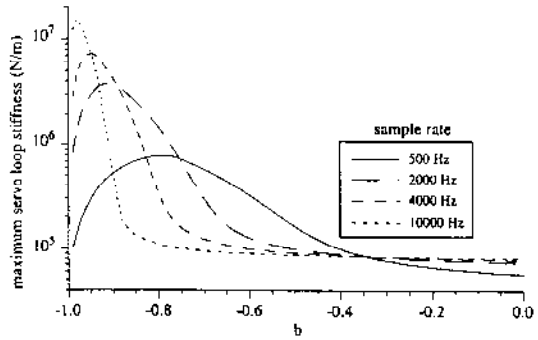

Fig. 8 Theoretical discrete PD control stiffness versus "b," $m = 17.40$ kg

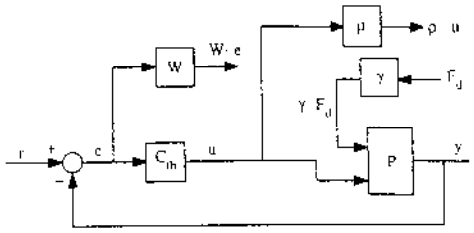

Fig. 9 H_∞ design setup block diagram

Several conclusions may be drawn from the data in Fig. 8. First, for the sampling rates shown here, the achievable stiffness using H_∞ control (on this particular linear motor system) is on the order of 10 to 100 times greater than is possible using PD control. Second, increasing the system mass yields an increase in achievable stiffness for both controller types. This is intuitive since mass acts as a low pass filter such that larger mass reduces the frequency response magnitude of the system, and therefore increases its stiffness. Finally, the effects of sampling rate are clearly visible: larger sample rate yields larger stiffness potential. Note however that the sensitivity of stiffness to sampling rate decreases with increasing sample rate, especially so for the optimal PD control curves.

4 Practical H_∞ Feedback Design

While Section 3 served to illustrate the dynamic stiffness potential of the H_∞ design method, it gave no consideration to robustness, control energy limits, closed-loop tracking properties, nor any other design aspect other than dynamic stiffness. Considering the unmodeled dynamics quantified by Fig. 6 as well as possible actuator saturation, it seems most unlikely that the H_∞ controllers obtained in the previous section will provide stability when implemented. This is in fact the case, and as such this section presents a more practical multi-objective H_∞ controller design.

As was the case for the SISO problem in the previous section, it is not the objective of this work to review in any depth the MIMO H_∞ problem nor its solution methods, both of which are well understood and well documented. A variety of commercial software packages now exist which perform the optimization, such as MATLAB μ-Tools from The MathWorks Inc., which was utilized in this research. For a complete treatment of the standard problem setup and background material, the reader is referred to (Maciejowski, 1989), or (Doyle et al., 1992).

The design setup used for this work is depicted in Fig. 9, and shows two inputs (r and F_d) and two outputs ($W \cdot e$ and $\rho \cdot u$). The selected inputs allow for the simultaneous consideration of both stiffness and tracking, with the scalar γ applying differential weighting between the two. The output $W \cdot e$ represents the frequency weighted combined output error from tracking r and from the force disturbance $\gamma \cdot F_d$. Finally, the output $\rho \cdot u$ represents a weighting on the control energy. Since H_∞ system norms are the induced norms of L_2 signals, this setup may loosely be thought of as minimizing a weighted sum of $e(t)^2 + u(t)^2$, although the actual transfer function norm being minimized for this MIMO system is not induced from this time domain signal. This setup has been converted to *standard form* in Fig. 10.

Since the MATLAB μ-Toolbox is designed for the continuous-time domain problem, discrete design has been accomplished using the w-plane transformation

$$w = \frac{2}{h}\frac{z-1}{z+1} \quad (8)$$

where h is the sampling period. This function maps the unit circle (closed unit disc) of the complex plane onto the imagi-

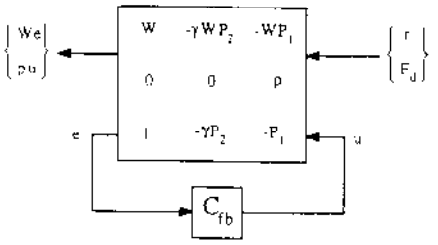

Fig. 10 H_∞ design setup in standard form

nary axis (closed left-half plane) of the complex plane. A stable system in the z-domain will thus have all of its poles in the open left-half of the w-plane after transformation. Since stability definitions in the w and s domains are identical, continuous-time domain design techniques may be applied to w-domain transformed discrete systems, with the w-domain controller transformed back into the z-domain as the final step. Further, this transformation is H_∞ norm preserving which justifies its use in discrete H_∞ design problems (Vidyasagar, 1985, p. 175).

The weighting filter $W(w)$ is chosen as a proper first order low-pass filter:

$$W(j\omega) = \frac{j\omega + 2\pi\beta_1}{j\omega + 2\pi\beta_2}, \quad \beta_1 > \beta_2 \tag{9}$$

This filter choice places greater tracking and stiffness emphasis on the low frequency range, desirable since the high frequency stiffness of the open loop plant is large to begin with, and also because good tracking performance is not in general required above some low frequency band. Note that the filter is chosen as proper, but not strictly proper. A strictly proper filter would, in order to satisfy the all-pass solution requirement, result in undesirable large controller gains at high frequency.

Two different H_∞ optimal controllers have been designed for the case of $m = 17.40$ kg. A sample rate of 2000 Hz was chosen for both, consistent with the fact that the open loop plant dynamics have been identified up to 1000 Hz (the Nyquist frequency for this sample rate).

Design A: $\rho = 1e-6$, $\gamma = 1e7$, $\beta_1 = 200$, $\beta_2 = 50$

$$C_{fb}(z) = 5.9867e5\,\frac{(z - 0.8197 + 0.0992i)(z - 0.8197 - 0.0992i)(z - 0.5773)}{(z - 0.8544)(z - 0.1561 + 0.4075i)(z - 0.1561 - 0.4075i)} \tag{10a}$$

Design B: $\rho = 1e-7$, $\gamma = 1e7$, $\beta_1 = 10$, $\beta_2 = 1$

$$C_{fb}(z) = 6.9214e5\,\frac{(z - 0.9690)(z - 0.8259)(z - 0.5778)(z + 0.9951)}{(z - 1)(z + 0.7538)(z + 0.0351 + 0.4278i)(z + 0.0351 - 0.4278i)} \tag{10b}$$

The weighting filter choice for design B places a tenfold emphasis on frequencies below 1 Hz as compared to those above 10 Hz, resulting in an integral action pole at $z = 1$ (to within four decimal places). The more moderate weighting in design A places this pole at $z = 0.8544$, providing large but finite D.C. controller gain. In comparison, the stiffness optimal PD controller at this sampling rate was determined to be:

$$C_{fb}(z) = 3.906e5\,\frac{z - 0.91}{z} \tag{10c}$$

Table 2 shows a comparison of the performance costs for each design criteria with each controller. One will notice that controller A is listed with a slightly suboptimal cost for the design A criteria. This is because it originally contained an additional zero-pole combination of $(z + 0.9905)/(z + 1)$ which was canceled since such a highly oscillatory controller mode could excite high frequency unmodeled dynamics. Controller A is also seen sub-optimal for criteria B by a similar slight amount, while controller B is more significantly suboptimal for criteria A by a factory of 1.6. In comparison, the optimal PD controller is suboptimal by a factor of 2.4 for criteria A, and 12.9 for criteria B.

Table 2 Controller performance costs for H_∞ design criteria

Controller	Design A criteria optimal cost = 1.1133	Design B criteria optimal cost = 0.2051
A	1.1185	0.2077
B	1.7867	0.2051
optimal PD	2.6577	2.6560

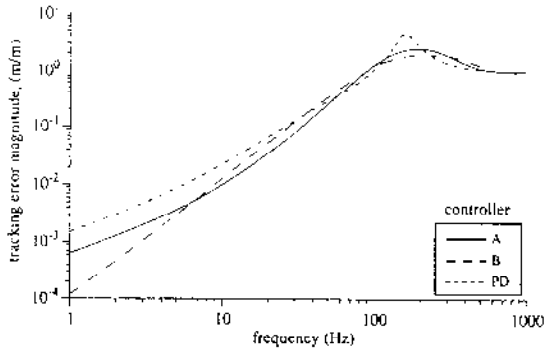

Fig. 11 Theoretical tracking error frequency responses

Tracking error frequency responses as predicted by the theoretical closed loop equations based on the nominal plant model are displayed in Fig. 11, and are seen qualitatively consistent with the weighting filter choices. The harmonic tracking performance of controller B is superior to design A for low frequencies up to 6 Hz, while controller A has the advantage for mid-range frequencies of 6 to 95 Hz. In comparison with the optimal PD controller, controller A provides better tracking up to 60 Hz, and controller B up to 30 Hz. The low frequency accuracy of these theoretical results has been experimentally verified at several frequencies, as tabulated in Table 3. These tests placed a considerable performance demand on the system: the ampli-

Table 3 Low frequency harmonic tracking error magnitude (m/m) (experimental value is listed above theoretical value)

Frequency (Hz)	Controller A	Controller B	Optimal PD
5	0.00294	0.00257	0.00683
	0.00364	0.00298	0.00856
10	0.00995	0.0106	0.0206
	0.00979	0.0126	0.0221
20	0.0344	0.0457	0.0635
	0.0345	0.0530	0.0671

Table 4 Dynamic stiffness of position feedback closed-loop system

Controller	Theoretical N/m	Experimental N/m	Hybrid N/m
A	5.5e6	3.3e6	3.2e6
B	5.0e6	3.8e6	3.4e6
optimal PD	3.8e6	2.6e6	3.8e6

tude of the reference sine wave was selected to require an rms inertial tracking force approximately equal to 70 percent of the 445 N continuous output capability of the linear motor.

Table 4 shows the experimentally determined closed loop dynamic stiffness by impact testing, with a PCB Electronics model 086C09 electric hammer providing a measurable impulsive disturbance to the system. Experimentally, controllers A and B are seen to improve dynamic stiffness by 27 and 46 percent, respectively, over the optimal PD controller. The column labeled "Theoretical" has been computed using the nominal system model given by (3). The "Hybrid" column takes into account the unmodeled system dynamics by computing (6) on a frequency by frequency basis with $P_1(z)$ replaced with experimentally based data (see Appendix). This calculation shows that the quantified unmodeled dynamics explain well the mismatch between theoretical and experimental dynamic stiffness for controllers A and B. This is further confirmed by examining the entire stiffness frequency response, shown in Fig. 12 for controller A. The hybrid computation in Table 4 is seen not as effective in the optimal PD case, possibly due to the omission of the $P_2(z)$ unmodeled dynamics.

5 H_∞ Optimal Force Feedback Design

Application of an outer force feedback control loop to the position feedback loop system provides a means of increasing dynamic stiffness beyond that achievable with position feedback only. One might arguably choose to call the controller force *feedforward*. However, force *feedback* has been used here since the cutting force is really a system output (from the cutting process), even though in Section 2 the cutting process was treated as external to the servo system for stability studies. In addition, there exists the possibility of instability in the force feedback loop, which is a trait characteristic of feedback, and not feedforward control. In any event, the terminology used is not of major importance.

The basic idea behind force feedback is this: sense the cutting force, and apply an equal and opposite actuator force to cancel it. If such a scheme could be perfectly implemented, the effects of the cutting process on the linear motor actuator would be completely eliminated. Of course, achievable loop bandwidths

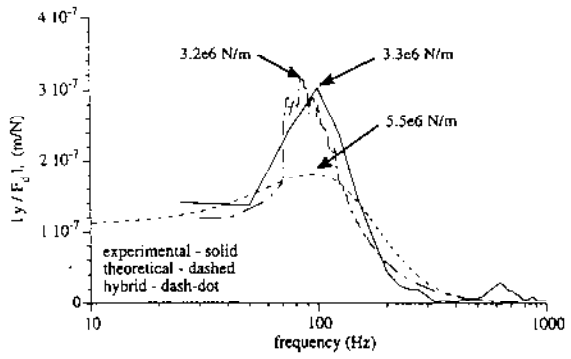

Fig. 12 Stiffness results for controller A

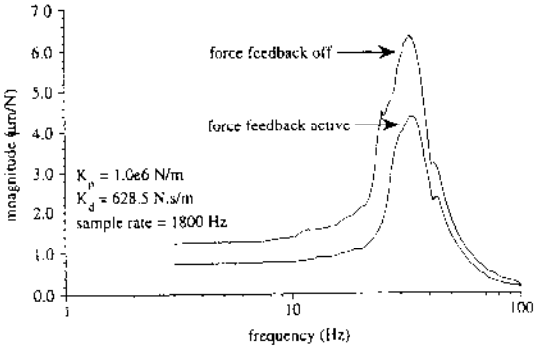

Fig. 13 Stiffness results for simple force feedback design

place a limitation on such an idealistic view. However, the bandwidth of the actuator force loop is not directly hampered by the system inertia, as is the case with position feedback. Its performance is instead primarily determined by the servo amplifier dynamics, which are considerably faster than those of the motor inertial system.

Implementation of force feedback control for machining requires the availability of the cutting force as a signal. One approach to sense this force is to mount the cutting tool post on a force dynamometer, and then affix this entire assembly to the (linear motor) feed drive slide (see Fig. 3). The structure dynamics of the tool post as well as those of the force sensor will be presently neglected, although they could be incorporated into the problem formulation if it were desired to do so. In particular, phase lag in the force sensor could significantly degrade closed loop performance, and might need to be accounted for if stiffness potentials are to be fully realized.

As motivation for the use of force feedback control in machining, a simple controller design of $C_{ffb} = 1$ was implemented

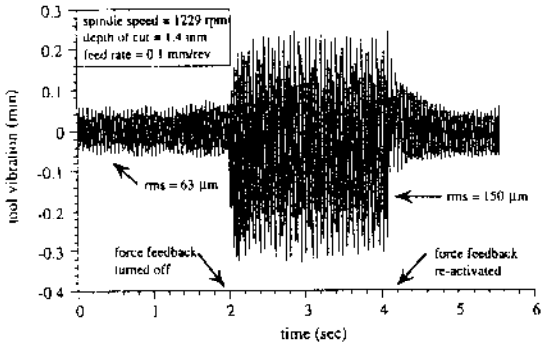

Fig. 14 Experimental cutting tool response for simple force feedback design

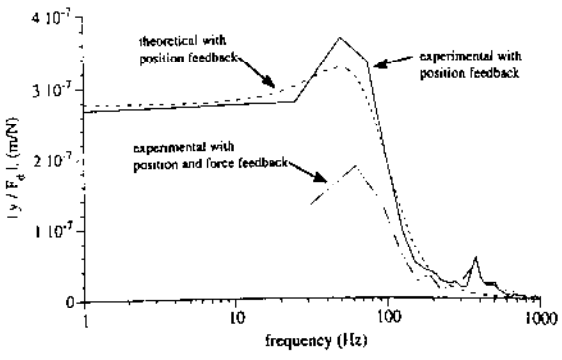

Fig. 15 Stiffness results for controller C

to augment the dynamic stiffness obtained from a (discrete equivalent) PD position feedback controller. The linear motor used for this is different from the one presented in Section 2, and the reader is referred to (Alter and Tsao, 1994 or 1993) for hardware, implementation, and metal cutting details. From Fig. 13, one may compute dynamic stiffness values of 2.3*e*5 N/m and 1.6*e*5 N/m respectively for the active and nonactive force feedback cases. Although both cases show low stiffness values, the addition of force feedback does yield a 44 percent dynamic stiffness improvement even with a simple negating compensation. Figure 14 shows the vibration of the linear motor (i.e., with cutting tool attached) during the axial configuration turning of a 416F stainless steel workpiece. Upon deactivating the force feedback controller (time $\approx$ 2 seconds), the tool is seen to immediately undergo unstable chatter vibrations, which are later suppressed by reactivating the force feedback controller. This demonstrates the utility of force feedback in machining.

In order to maximize the dynamic stiffness using force feedback, the control goal is again to minimize the H_∞ norm of the transfer function y/F_c. The closed-loop transfer function from cutting force to position is computed from Fig. 2 and Eq. (5)

$$\frac{y}{F_c} = \frac{-P_2}{1 + P_1C_{fb}} + C_{ffb}\frac{P_1}{1 + P_1C_{fb}}. \tag{11}$$

This is already in standard model matching form, and directly gives the optimal cost function

$$J_\infty^{\text{opt}} = \inf_{Q \in R_\infty} \|M - GQ\|_\infty \tag{12}$$

where $Q := -C_{ffb}$, and $M, G \in R_\infty$ are defined as $M := -P_2/(1 + P_1C_{fb})$, $G := P_1/(1 + P_1C_{fb})$. As in Section 3, the optimization problem (12) has again been solved via simple interpolation.

When G in (12) contains one or more unit circle zeros, the optimal solution Q^{opt} may not exist. One solvable special case is where every unit circle zero of G is also a zero of M. In this case, a solution may be found by solving a sequence of problems where the unit circle zeros are perturbed to the stable region, with the perturbations converging to zero (Vidyasagar, 1985, pp. 174–178). With the practically importance case where the position feedback controller has been designed with integral action in mind, one sees that those unit circle zeros of G obtained from unit circle poles of C_{fb} are also common to M, and therefore do not hinder the solvability of the problem.

The addition of the force dynamometer adds additional mass to the linear motor system, as was documented in Section 2. As such, the position feedback controllers presented in Section 4 were first redesigned to account for this change:

Design C: $\rho = 1e-5$, $\gamma = 1e7$, $\beta_1 = 200$, $\beta_2 = 50$

$$C_{fb}(z) = 2.1733e5\,\frac{(z - 0.8687 + 0.0482i)(z - 0.8687 - 0.0482i)(z - 0.5730)}{(z - 0.8544)(z - 0.4676 + 0.2956i)(z - 0.4676 - 0.2956i)} \tag{13a}$$

Design D: $\rho = 1e-6$, $\gamma = 1e7$, $\beta_1 = 10$ $\beta_2 = 1$

$$C_{fb}(z) = 2.5319e5\,\frac{(z - 0.9683)(z - 0.9018)(z - 0.5731)}{(z - 1)(z - 0.4297 + 0.3191i)(z - 0.4297 - 0.3191i)} \tag{13b}$$

Similar to the two controllers designed in Section 4, controller D has integral action while controller C does not. However, the above controller gains have been limited to a greater extent by the larger unmodeled dynamics present with this higher mass case, possibly due to the flexibility of the dynamometer. They therefore offer less dynamic stiffness than was achieved for the lower mass case. The experimental dynamic stiffness values determined by impact test, respectively for controllers C and D, are 2.7*e*6 and 3.2*e*6 N/m, compared to the theoretical prediction of 3.1*e*6 and 2.9*e*6 N/m.

Force feedback controllers were designed using (12), and are given by the following transfer functions:

For Design C:

$$C_{ffb}(z) = \frac{(z - 0.5661)(z - 0.4839 + 0.3055i)(z - 0.4839 - 0.3055i)(z - 0.1883)}{z(z - 0.4676 + 0.2956i)(z - 0.4676 - 0.2956i)(z + 0.2307)} \tag{14a}$$

For Design D:

$$C_{ffb}(z) = \frac{(z - 0.561)(z - 0.4488 + 0.3289i)(z - 0.4488 - 0.3289i)(z - 0.1847)}{z(z - 0.4297 + 0.3191i)(z - 0.4297 - 0.3191i)(z + 0.2307)} \tag{14b}$$

The force feedback controller for Design C originally contained an additional zero-pole combination of $(z - 0.8546)/(z - 0.8544)$ and produced a theoretical all-pass stiffness value of 5.5*e*8 N/m. After removal of this pair, the theoretical closed loop dynamic stiffness was reduced by 11 percent to 4.9*e*8 N/m.

The force feedback controller for Design D originally contained an additional zero-pole combination of $(z - 1.0002)/(z - 1)$, and yielded a theoretical all-pass stiffness value of 5.5*e*8 N/m. This unit circle pole results directly from the integral action of the feedback controller D, such that G in (12) contained a unit circle zero at $z = 1$ which was perturbed into the stable region during the solution computation, with the perturbation later being reduced to zero as the last step. Cancellation of this pair reduced this dynamic stiffness value by 14 percent to 4.7*e*8 N/m. In the general case, a similar zero may not exist with which to cancel such unit circle poles. They must instead be left perturbed in the stable region, which will also result in a reduction of stiffness. For example, had the above pole at $z = 1$ been perturbed to $z = 0.99$ (and the zero at $z = 1.0002$ left intact), the resulting theoretical dynamic stiffness would be 1.1*e*7, or a reduction of 98 percent! In addition, while $z = 0.99$ may be theoretically stable, it may not provide adequate performance from a practical point of view. Such difficulties must be solved through engineering judgment on case by case basis.

The zero-pole cancellations and perturbations discussed above illustrate the sensitivity of dynamic stiffness to even small dynamic mismatches between the force feedback controller and

the servo loop. Owing to the unmodeled dynamics here present in the open loop linear motor, it might be anticipated that experimental dynamic stiffness will not achieve a level comparable with theoretical values. This in fact turns out to be the case, although stiffness improvements are still provided. Experimental stiffness was determined through impact testing, as shown in Fig. 15 for design C. One sees that the addition of force feedback to design C experimentally yields a dynamic stiffness of 5.4*e*6 N/m: a two fold increase over the 2.7*e*6 N/m value using position feedback alone. For design D (figure not shown), force feedback also produces a dynamic stiffness of 5.4*e*6 N/m, for a 70% increase over the position feedback only value of 3.2*e*6 N/m.

6 Conclusion

The potential of the H_∞ methodology when designing for dynamic stiffness has been demonstrated. The theoretically achievable stiffness using H_∞ control is for the present hardware on the order of 10 to 100 times larger than that obtainable with conventional PD control. For implementation purposes, a practical H_∞ design was employed which considered not only stiffness but also robust stability and tracking and control energy. One design setup was also chosen to yield a position feedback controller with integral action properties; a desirable feature for machine tools. Experimental dynamic stiffness gains over PD control of 27 to 46 percent have been shown. Finally, the use of H_∞ optimal force feedback control for stiffness enhancement was also experimentally demonstrated, resulting in a 70–100 percent dynamic stiffness increase over position feedback alone.

The software currently available to assist with H_∞ controller design is extensive in scope. As such, this technique offers an attractive practical alternative to conventional PD control for direct feed drive stiffness design. More extensive modeling of the linear motor and power amplifier may be needed to fully exploit the stiffness potential of linear motor feed drives. In addition, careful planning of the mechanical design of the feed drive should be performed to eliminate large structural resonance and excessive amounts of friction, and thereby reduce the unmodeled system dynamics.

References

Alter, D. M., 1994, *Control of Linear Motors for Machine Tool Feed Drives*, Ph.D. dissertation, Univ. of Illinois at Urbana-Champaign.

Alter, D. M., and Tsao, T-C, 1995, "Control of Linear Motors for Machine Tool Feed Drives: Optimal Feedforward Control for Tracking Improvement" submitted for publication, ASME JOURNAL OF DYNAMIC SYSTEMS, MEASUREMENT, AND CONTROL.

Alter, D. M., and Tsao, T-C, 1994, "Stability of Turning Processes with Actively Controlled Linear Motor Feed Drives," ASME *Journal of Engineering for Industry*, Vol. 116, No. 3, pp. 298–307.

Doyle, J. C., Francis, B. A., and Tannenbaum, A. R., 1992, *Feedback Control Theory*, Macmillan Publishing, New York.

Franklin, G. F., and Powell, J. D., 1981, *Digital Control of Dynamic Systems*, Addison-Wesley Publishing Co., Reading, MA, pp. 85–92.

Maciejowski, J. M., 1989, *Multivariable Feedback Design*, Addison-Wesley, Reading, MA, pp. 265–324.

Merritt, H. E., 1965, "Theory of Self-Excited Machine Tool Chatter," ASME *Journal of Engineering for Industry*, Vol. 87, No. 4, pp. 447–454.

Srinivasan, K., and Nachtigal, C. L., 1978, "Analysis and Design of Machine Tool Chatter Control Systems Using the Regenerative Spectrum," ASME JOURNAL OF DYNAMIC SYSTEMS, MEASUREMENT, AND CONTROL, Vol. 100, pp. 191–200.

Vidyasagar, M., 1985, *Control System Synthesis: A Factorization Approach*, The MIT Press, Cambridge, MA.

Zames, G., and Francis, B. A., 1983, "Minimax Sensitivity, and Optimal Robustness," *IEEE Transactions on Automatic Control*, Vol. 28, pp. 585–601.

APPENDIX

Computation of "Hybrid" Stiffness

Suppose that the unmodeled dynamics of the open-loop plant are characterized in the discrete-time domain as:

$$\hat{P}_1(z) = P_1(z)[1 + \Delta_1(z)] \tag{15}$$

where $\hat{P}_1(z)$ is the actual plant, $P_1(z)$ is the nominal plant, and $\Delta_1(z)$ is a stable multiplicative perturbation. The "Hybrid" computation is to be performed by replacing $P_1(z)$ with $\hat{P}_1(z)$ in Eq. (6). However, the system unmodeled dynamics are currently known only in the continuous-time domain (i.e., see Fig. 6), and therefore some conversion to discrete-time is needed. Given an arbitrary stable continuous-time domain system transfer function $H(s)$ with complex frequency response $H(j\omega)$, one may express the frequency response of its discrete zero-order hold equivalent as (Franklin and Powell, 1981):

$$H(z)|_{z=e^{j\omega h}} = (1 - e^{-j\omega h}) \frac{1}{h} \sum_{n=-\infty}^{n=+\infty} \frac{H(j\omega - jn\omega_s)}{j\omega - jn\omega_s} \tag{16}$$

where h is the sampling period and $\omega_s = 1/(2\pi h)$. However, if $H(j\omega)$ is zero for all frequencies above $\omega_s/2$, (16) reduces to

$$H(z)|_{z=e^{j\omega h}} = (1 - e^{-j\omega h}) \frac{1}{h} \frac{H(j\omega)}{j\omega}. \tag{17}$$

Now, the continuous-time complex frequency response $\hat{P}_1(j\omega)$ was experimentally determined at distinct frequencies up to 1000 Hz (i.e., $\omega_s/2$). Referring to Fig. 5, it is arguably reasonable to take as zero the diminishing frequency response above 1000 Hz. Thus, (17) may be used to compute (approximately) the complex frequency response of $\hat{P}_1(e^{j\omega h})$ on a frequency by frequency basis.